First-Principles Studies of Er_2O_3(110) Heteroepitaxy on Si(001)

Yen-Wei Chen, Po-Liang Liu, and Chun-Hsiang Chan

***Abstract*—We present first-principles total-energy density functional calculations to study the heterojunction between a cubic Er_2O_3(110) film and Si(001) substrate. Using repeated free-surface terminated slabs, the relative stability of eight different models of the Er_2O_3(110)/Si(001) interface is examined as their interfacial energies and bonding analyses. The most favorable interface consists of the fourfold-coordinated Si with one Er-Si, one O-Si and two Si-Si bonds, with two Er-Si and two Si-Si bonds, and with two O-Si and two Si-Si bonds. Our findings show that the Si-Si and Er-O bond lengths immediately adjacent to the interface layer are slightly expanded and alternately released in compression and tension relative to their bulk values, respectively. Our findings agree with previously reported experimental results.**

***Index Terms*—Er_2O_3, Si, interface, first-principles calculations.**

I. Introduction

Rare earth oxides (REOs) thin films open up new doors in the development of important devices across a variety of special advantages such as the high dielectric consatant, good thermodynamic stability, and wide band gap. The REOs thin films such as Y_2O_3, Pr_2O_3, La_2O_3, and Er_2O_3 films have gained great attentions and their applications have become a hot and active field in the world range wide [1], [2]. For example, R. L. Nigro *et al.* showed that Pr_2O_3 films grown epitaxially on Si(100) substrates were prepared via metal–organic chemical vapor deposition (MOCVD) and found to be comprised of a praseodymium silicate interfacial layer increased as the postannealing temperature rose [1]. The erbium (III) oxide (Er_2O_3) thin film is one of the most stable REOs thin films even for use at postannealing temperature in the range from 600 ℃ to 900 ℃ [2], which showed that the interfacial Si–O–Er bonds in Er_2O_3/Si heteroepitaxial structures are formed by a reaction with Si atoms diffusing from the substrate [2]. Er_2O_3 alloys have a cubic fluorite-related bixbyite structure and lattice constant of 10.55 Å which closely matches the value 10.86 Å found experimentally in Si [3]. Therefore, it is expected that the Er_2O_3 thin films could be epitaxially grown on Si substrates. S. Chen *et al.* demonstrated that Er_2O_3 thin films grown on Si (111) substrates show poorer thermal stability than those grown on Si(001) substrates [4]. Furthermore, R. Xu *et al.* reported that the epitaxial growth of Er_2O_3 films grown by molecular beam epitaxy (MBE) on Si (001) substrates are characterized by the relationship: Er_2O_3(110)/Si(001), Er_2O_3[001]/Si[110], and Er_2O_3[-110]/Si[110] [5]. However, no work has been down on theoretical mechanism for the heterojunction of the Er_2O_3(110)/Si(001). In this work, we not only present the optimized Er_2O_3(110)/Si(001) heterostructure but also provide the thermoelastic properties of the interface structure.

Manuscript received November 9, 2013; revised January 16, 2014.

The authors are with National Chung-Hsing University, Taiwan (e-mail: pliu@dragon.nchu.edu.tw).

II. Theoretical Approach

We undertook a series of *ab initio* calculations to study the energetic and structural properties of various Er_2O_3(110)/Si(001) heterostructures. Our first-principles results were obtained using the Vienna *Ab Initio* Simulation Package (VASP) [6]-[8], which utilize Vanderbilt ultrasoft pseudopotentials (USPPs) to efficiently treat ion-electron interactions. This program employed USPPs derived from the projector augmented wave (PAW) method and the generalized gradient approximation (GGA) with the Perdew-Wang (PW91) exchange-correlation functional [9], [10]. The electronic configurations for the valence electrons are Er: $4f^{12}6s^2$, O: $2s^22p^4$, and Si: $3s^23p^2$. The values of the chemical potentials of Er_2O_3 ($\mu_{Er_2O_3}^{bulk}$), Er (μ_{Er}), O (μ_O), and Si (μ_{Si}) are determined from the total energies per atom of bulk Er_2O_3 (space group: 206 *Ia-3*), bulk Er (space group: 194 *P63/MMC*), gas O_2 (space group: 123 *P4/mmm*), and bulk Si (space group: 227 *FD3-MS*), respectively. The adhesion energy ($E_{slab}^{Er_2O_3/Si}$) of the isolated Er_2O_3 to Si slabs is used to approximate the interface energy [11] given by

$$E_{slab}^{Er_2O_3/Si} = n_{Er}\ \mu_{Er} + n_O\ \mu_O + n_{Si}\ \mu_{Si} + A[\sigma^{Er_2O_3}(\mu_{Er}) + \sigma^{Si}(\mu_{Si})] + A\,\Gamma_m, \quad (1)$$

where Γ_m denoted by model number m is the Er_2O_3-Si interfacial energy and A is the surface area The number of atoms of Er, O, and Si are given by n_{Er}, n_O, and n_{Si}, respectively. The chemical potentials of Er and O in Er_2O_3 are given by μ_{Er} and μ_O while this of Si is given by μ_{si}. The surface energy terms, $\sigma^{Er_2O_3}$ and σ^{Si}, account for two equivalent surfaces in each slab for Er_2O_3 and Si through the equation

$$\sigma = (E_{slab} - \sum_i n_i\ \mu_i)/(2A). \quad (2)$$

Here, E_{slab} is the total energy of the particular slab; and n_i

and μ_i are the number of atoms and the chemical potential of the *i*th constituent of the slab. The factor of 2 accounts for two equivalent surfaces in the particular slab.

TABLE I: BONDING ANALYSES OF MODELS 1–8 SHOWN IN FIG. 1 EACH MODEL HAS SIX BONDS DOMINATED BY THREE MAIN ANALOGUES, WHICH ARE REFERRED TO AS THE ER–SI–ER, O–SI–O, AND ER–SI–O BONDING ENVIRONMENTS

	Modle1	Modle2	Modle3	Modle4	Modle5	Modle6	Modle7	Modle8
Er-Si-Er	0	1	1	1	1	2	1	2
O-Si-O	0	0	0	0	0	1	0	0
Er-Si-O	6	5	5	5	5	3	5	4

To discuss quantitatively the interface energy between Er_2O_3 and Si slabs, we have employed repeated slab geometry with separated Er_2O_3 and Si slab with free surfaces. The total energy of isolated Er_2O_3 and Si slabs (with free surfaces) can be written as

$$E_{slab}^{Er_2O_3} = n_{Er}\,\mu_{Er} + n_O\,\mu_O + 2A\,\sigma^{Er_2O_3}(\mu_{Er}) \quad (3)$$

and

$$E_{slab}^{Si} = n_{Si}\,\mu_{Si} + 2A\,\sigma_{Si}(\mu_{Si}). \quad (4)$$

Subtracting Eqs (3) and (4) form Eq. (1) we obtain

$$\Delta E_{slab} = E_{slab}^{Er_2O_3/Si} - E_{slab}^{Er_2O_3} - E_{slab}^{Si}. \quad (5)$$

ΔE_{slab} approximates the work of adhesion of isolated Er_2O_3 and Si slabs (with free surface) and is related to the interface energy Γ_m through the equation

$$\Gamma_m(\mu_{Er}, \mu_{Si}) = \Delta E_{slab}/A + \sigma^{Er_2O_3}(\mu_{Er}) + \sigma_{Si}(\mu_{Si}). \quad (6)$$

With this approach, all atomic positions are allowed to relax fully in a supercell of fixed dimensions in each of the structural models corresponding to the joined and isolated slabs, yielding $E_{slab}^{Er_2O_3/Si}$, $E_{slab}^{Er_2O_3}$, and E_{slab}^{Si} slabs , respectively.

Eight interface models with specific bonding arrangements between Er_2O_3(110)/Si(001), Er_2O_3[001]/Si[110], and Er_2O_3[-110]/Si[110] were first constructed using bulk crystalline configurations as shown in Fig. 1. From Fig. 1, we have examined eight types of interface: In Model 1, the interface with the fourfold-coordinated Si consists of a Si atom bonded to one Er and O atom and two Si atoms, denoted here by the Er–Si–O bonding environment; in Models 2–5, 7, and 8, the interface with the fourfold-coordinated Si consists of the Er–Si–O bonding environment, and a Si atom bonded to two Er and Si atoms, denoted here by the Er–Si–Er bonding environment; in Model 6, the interface with the fourfold-coordinated Si consists of the Er–Si–O and Er–Si–Er bonding environments, and a Si atom bonded to two O and Si atoms, denoted here by the O–Si–O bonding environment. To further clarify the bonding environment described in Fig. 1 we also present atomic structures of the interface in Fig. 2(a)–Fig. 2(c), for the Er–Si–Er, O–Si–O, and Er–Si–O bonding environment, respectively. Table I lists the results of our bonding analyses for 8 models in Fig. 1. The stoichiometry of eight heterostructures was fixed at $Er_{32}O_{48}Si_{48}$.

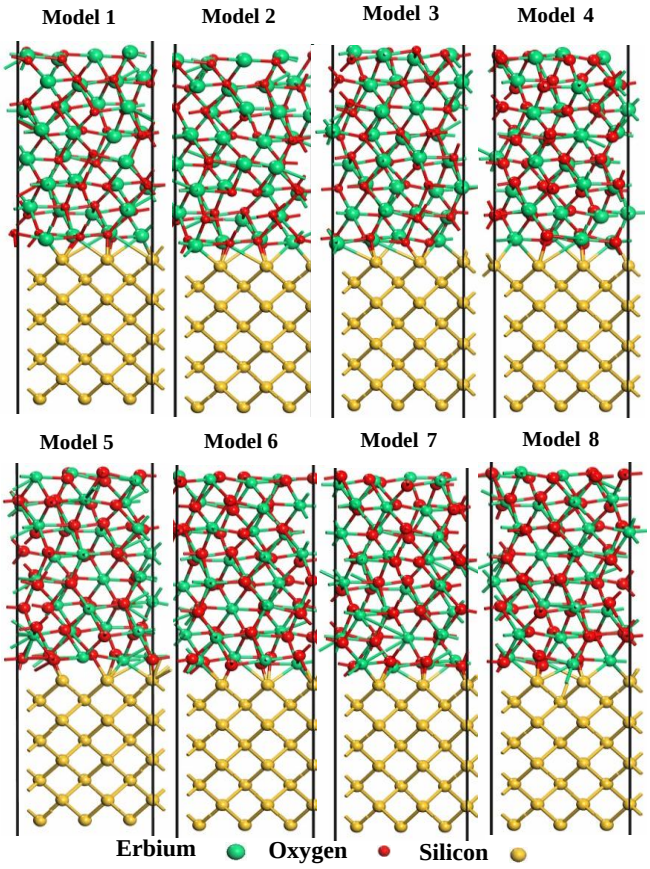

Fig. 1. Ball and stick structural representations of the eight interface configuration models considered in this study. The atoms are represented by spheres: Er (green, large), O (red, small), and Si (yellow, medium).

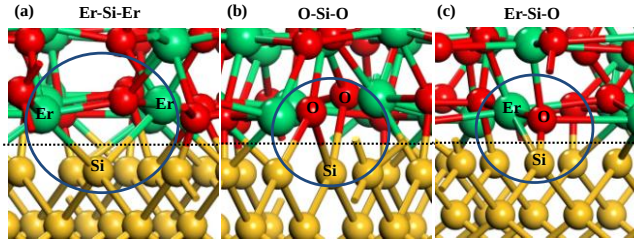

Fig. 2. Ball and stick structural representations of (a) Er–Si–Er, (b) O–Si–O, and (c) Er–Si–O bonding environments on Er2O3/Si interfaces considered in this study. The dashed line is the interface. The atoms are represented by spheres: Er (green, large), O (red, small), and Si (yellow, medium).

III. RESULTS AND DISCUSSION

The structurally optimized interface models relaxed to their zero force positions are shown in Fig. 3. The Er_2O_3/Si interface energy Γ_m as defined by Eq. (1) is a bilinear function of the chemical potentials μ_{Er} and μ_{Si}. The calculated interface energies for Models 1–8 are –0.01, –0.11, –0.01, –0.01, –0.11, –0.11, –0.01, and 0.02

eV/Å^2. Models 2, 5 and 6 have the lowest overall energy of –0.11 eV/Å^2, with interface structures consisting of one Er–Si–Er and five Er–Si–O bonding environments for Models 2 and 5, and two Er–Si–Er, one O–Si–O, and three Er–Si–O bonding environments for Model 6 (see Table I). Models 1, 3, 4, and 7 are the second most favorable interface structures with interfacial energies of –0.01 eV/Å^2. Model 8 is unstable or metastable, with $\Gamma_8 > 0$.

TABLE II: PERCENT DEVIATIONS OF NEAR-INTERFACE BOND LENGTHS FROM THEIR CORRESPONDING BULK VALUES FOR MODELS 1–8

	$\Delta d^1_{Si\text{-}Si}/d^{bulk}_{Si\text{-}Si}$	$\Delta d^2_{Si\text{-}Si}/d^{bulk}_{Si\text{-}Si}$	$\Delta d^1_{Er\text{-}O}/d^{bulk}_{Er\text{-}O}$	$\Delta d^2_{Er\text{-}O}/d^{bulk}_{Er\text{-}O}$
Model 1	1.60%	1.03%	5.21%	7.76%
Model 2	1.45%	0.93%	9.86%	13.2%
Model 3	1.06%	0.82%	9.85%	8.96%
Model 4	1.03%	0.99%	11.79%	9.99%
Model 5	1.54%	1.01%	10.56%	9.91%
Model 6	1.30%	0.90%	-1.53%	6.23%
Model 7	1.31%	0.74%	2.26%	6.65%
Model 8	5.64%	3.89%	1.14%	3.01%

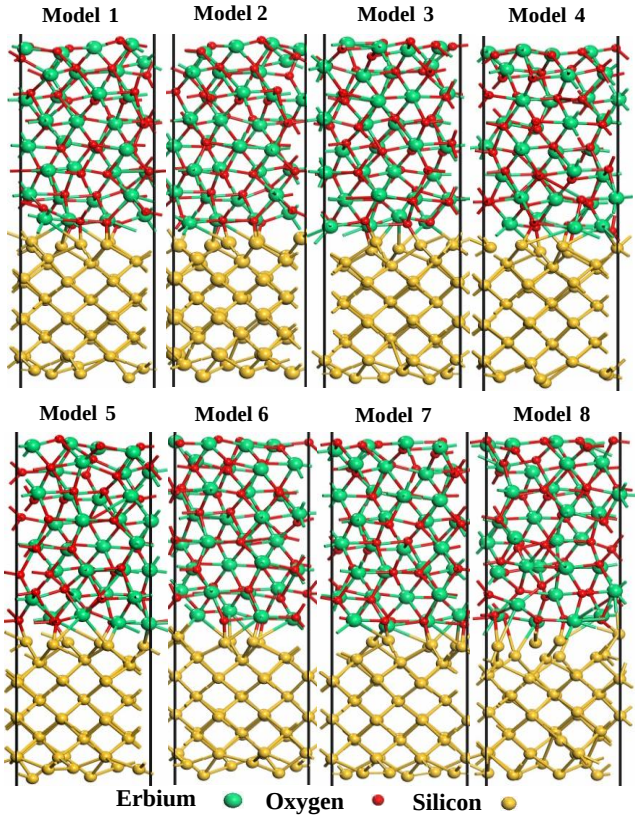

Fig. 3. Ball and stick structural representations of the eight optimized interface configuration models considered in this study. The atoms are represented by spheres: Er (green, large), O (red, small), and Si (yellow, medium).

The Superscripts "1" and "2" in the ratios Δd/d denote bond lengths within the first and second layers on either side of the interface. $\Delta d^1_{Si\text{-}Si}/d^{bulk}_{Si\text{-}Si}$, $\Delta d^2_{Si\text{-}Si}/d^{bulk}_{Si\text{-}Si}$, $\Delta d^1_{Er\text{-}O}/d^{bulk}_{Er\text{-}O}$, and $\Delta d^2_{Er\text{-}O}/d^{bulk}_{Er\text{-}O}$ are the innermost and second Si–Si and Er–O bond lengths, respectively

Further insight into the strain relaxation near the interfaces of Er_2O_3(110)/Si(001) heterostructures can be obtained by examining the deviations of the bond length adjacent to the interface from their bulk values as shown in Table II. We carry out a detailed comparison of the bond lengths obtained from the bond lengths adjacent to the interface and their bulk values calculated from optimized unit cells. It can be observed in Table II that Model 6 has the smallest bond strains. In Model 6, the Si–Si bond lengths adjacent to the interface are slightly expanded relative to their bulk values calculated from optimized unit cells ($\Delta d^1_{Si\text{-}Si}/d^{bulk}_{Si\text{-}Si}$ = 1.30% and $\Delta d^2_{Si\text{-}Si}/d^{bulk}_{Si\text{-}Si}$ = 0.90%), while the Er–O bond lengths adjacent to the other side of the interface are alternately released in compression and tension ($\Delta d^1_{Er\text{-}O}/d^{bulk}_{Er\text{-}O}$ = –1.53% and $\Delta d^2_{Er\text{-}O}/d^{bulk}_{Er\text{-}O}$ = 6.23%). Our results for the bond length analyses show that Model 6 is the most favorable bonding arrangement within two Er–Si–Er, one O–Si–O, and three Er–Si–O bonding environments, suggesting a possible explanation in a largest bond relaxations due to the presence of the O–Si–O bonding environments (not shown in Models 1–5, 7, and 8). Our results in Fig. 3, Tables I, and II corroborate the X-ray diffraction (XRD) observations of Er_2O_3(110) layers grown by MBE on Si(001) substrates, indicating that the surface treatment of O-exposure on the upper Si templates to form the O–Si–O bonding environments, the O-rich conditions, can degrade the Er-silicide formation, form Er- and Si-oxide in the interface, and achieve good epitaxial growth of Er_2O_3(110) films on Si(001) [5].

The second lowest interfacial bond strain is Model 7 as shown in Table II. In Model 7, the Si–Si bond lengths adjacent to the interface are slightly expanded relative to their bulk values calculated from optimized unit cells ($\Delta d^1_{Si\text{-}Si}/d^{bulk}_{Si\text{-}Si}$ = 1.31% and $\Delta d^2_{Si\text{-}Si}/d^{bulk}_{Si\text{-}Si}$ = 0.74%), while the Er–O bond lengths adjacent to the other side of the interface exhibit large artificial tensile strains ($\Delta d^1_{Er\text{-}O}/d^{bulk}_{Er\text{-}O}$ = 2.26% and $\Delta d^2_{Er\text{-}O}/d^{bulk}_{Er\text{-}O}$ = 6.65%). Apart from Model 6, Models 2 and 5 are the most favorable interface geometries with interfacial energies of –0.01 eV/Å^2. In Model 2, the Si–Si bond lengths adjacent to the interface are slightly expanded relative to their bulk values calculated from optimized unit cells ($\Delta d^1_{Si\text{-}Si}/d^{bulk}_{Si\text{-}Si}$ = 1.45% and $\Delta d^2_{Si\text{-}Si}/d^{bulk}_{Si\text{-}Si}$ = 0.93%), while the Er–O bond lengths adjacent to the other side of the interface exhibit large artificial tensile strains ($\Delta d^1_{Er\text{-}O}/d^{bulk}_{Er\text{-}O}$ = 9.86% and $\Delta d^2_{Er\text{-}O}/d^{bulk}_{Er\text{-}O}$ = 13.22%). In Model 5 similar to the Model 2, having Er–Si–Er and Er–Si–O bonding environments as listed in Table I, the Si–Si bond lengths adjacent to the interface are slightly expanded relative to their bulk values calculated from optimized unit cells ($\Delta d^1_{Si\text{-}Si}/d^{bulk}_{Si\text{-}Si}$ = 1.54% and $\Delta d^2_{Si\text{-}Si}/d^{bulk}_{Si\text{-}Si}$ = 1.01%), while the Er–O bond lengths adjacent to the other side of the interface exhibit large artificial tensile strains ($\Delta d^1_{Er\text{-}O}/d^{bulk}_{Er\text{-}O}$ = 10.56% and $\Delta d^2_{Er\text{-}O}/d^{bulk}_{Er\text{-}O}$ = 9.91%). Both models, Models 2 and 5, have the most favorable interface energies (–0.11 eV/Å^2) but they do not have low bond strains. The other three models, i.e., Models 1, 3, and 4, are the same low interface energies (–0.01 eV/Å^2), which in turn resulted in high bond strains. Furthermore, Model 8 has the highest interface energies (0.02 eV/Å^2), that lead to highest tensile strains

($\Delta d^1_{Er\text{-}O}/d^{bulk}_{Er\text{-}O}$ = 5.64% and $\Delta d^2_{Er\text{-}O}/d^{bulk}_{Er\text{-}O}$ = 3.89%).

From our *ab initio* calculations, we have determined that the most favorable interfacial bonding geometry (Model 6, Fig. 2) contains two Er–Si–Er, one O–Si–O, and three Er–Si–O bonding environments. To compare the interfacial bonding arrangement of Models 1–8, $Er_2Si_2O_7$ and $ErSi_2$ were calculated to elucidate a mechanism for mismatch accommodation between the Er_2O_3(110) films and Si(001) templates. We obtained relaxed lattice constants a = 4.68 Å, b = 5.56 Å, and c = 10.79 Å for the equilibrium structure of $Er_2Si_2O_7$ (space group: 14 *P21/c*), while $a = b$ = 3.79 Å and c = 4.08 Å are determined from the equilibrium structure of $ErSi_2$ (space group: 191 *P6/mmm*). Table III represents the ratio between the Si-O (Er-Si) bond lengths immediately adjacent to the interface in Models 1–8 and the Si-O (Er-Si) bond lengths of $Er_2Si_2O_7$ ($ErSi_2$). From Table III, it can be seen that Model 6 has the smallest bond strains, which show that the Si-O and Er-Si bond lengths immediately adjacent to the interface layer are expanded (6.64%) and compressed (0.30%) relative to those of $Er_2Si_2O_7$ and $ErSi_2$, respectively. The smaller bond strains in Model 6 are consistent with its more favorable bonding arrangement. Apart from Model 6, the other five models, i.e., Models 2, 3, 4, 5, and 7, are similar except that the Si-O and Er-Si bond lengths exhibit a larger tensile and compressed strain (see Table III), respectively. In the case of Model 2, the Si-O and Er-Si bond lengths immediately adjacent to the interface layer are expanded (8.04%) and compressed (6.92%) relative to those of $Er_2Si_2O_7$ and $ErSi_2$, respectively. Similarly, in Model 5, the Si-O and Er-Si bond lengths immediately adjacent to the interface layer are expanded (7.64%) and compressed (8.37%) relative to those of $Er_2Si_2O_7$ and $ErSi_2$, respectively. In contrast to Models 2–7, Model 1 exhibits the largest bond strains, which show that the Si-O bond lengths immediately adjacent to the interface layer are expanded (16.16%) relative to those of $Er_2Si_2O_7$. In the bond length analysis for Models 2–5, 7, and 8 as seen in Table I and III, it can be clearly seen that Si-O bond strains increase with decreasing the number of interfacial Er–Si–O bonds and Er-Si bond strains undergo a transition from compressed to tensile strain with increasing the number of interfacial Er–Si–Er bonds. Our results indicate that interfacial Er–Si–O bonds are more desirable than Er–Si–Er that cause degradation of key thermoelastic properties at the film/substrate interfaces, in excellent agreement with recent experimental evidence of erbium oxide films grown by laser MBE on Si(001) surfaces[12].

TABLE III: PERCENT DEVIATIONS OF NEAR-INTERFACE SI-O AND ER-SI BOND LENGTHS FROM THE CORRESPONDING BOND LENGTHS OF BULK ER2SI2O7 AND ERSI2, RESPECTIVELY

	Si-O	Er-Si
Model 1	16.16%	-
Model 2	8.04%	-6.92%
Model 3	8.24%	-4.36%
Model 4	8.27%	-8.15%
Model 5	7.64%	-8.37%
Model 6	6.64%	-0.30%
Model 7	8.83%	-2.57%
Model 8	9.201%	2.22%

IV. CONCLUSIONS

The interface energies of Er_2O_3(110) films grown epitaxially on the Si(001) substrates were studied by first-principles calculations. By studying the thermodynamic stability of eight interface structural models with a fixed $Er_{32}O_{48}Si_{48}$ stoichiometry and comparing their interface energies, we found that Models 2, 5, and 6 have the lowest interface energy. By comparing the bond lengths adjacent to the Er_2O_3(110)/Si(001) interface, we found that Model 6 has the largest bond relaxations within two Er–Si–Er, one O–Si–O, and three Er–Si–O bonding environments. Our result agrees with recent MBE experiments on Er_2O_3(110) films epitaxially grown on Si(001) substrates.

ACKNOWLEDGMENT

This work was supported by the National Science Council under contract no. NSC102-2221-E-005-030 and in part by the Ministry of Education, Taiwan under the ATU plan. Computational studies were performed using the resources of the National Center for High Performance Computing.

REFERENCES

[1] R. L. Nigro, R. G. Toro, G. Malandrino, G. G. Condorelli, V. Raineri, and I. L. Fragalà, "Pradeodymium Silicate as a High-k Dielectic Candidate: An insight into the Pr_2O_3-Film/Si-Substrate Interface Fabricated Though a Metal-Organic Chemical Vaapor Deposition Process," *Adv. Funct. Mater*, vol. 15, pp. 838-845, May 2005.

[2] H. Ono and T. Katsumata, "Interfacial reactions between thin rare-earth-metal oxide films and Si substrates," *Appl. Phys. Lett.*, vol. 78, pp. 1831-1834, March 2001.

[3] Y. Y. Zhu, R. Xu, S. Chen, Z. B. Fang, F. Xue, Y. L. Fan, X. J. Yang, and Z. M. Jiang, "Epitaxial growth of Er2O3 films on oxidized Si(111) and Si(001) substrates," *Thin Solid Films*, vol. 508, pp. 86-89, November 2006.

[4] S. Chen, Y. Zhu, R. Wu, Y. Wu, Y. Fan, and Z. Jianga, "Thermal stability of Er_2O_3 thin films grown epitaxially on Si substrates," *J. Appl. Phys.*, vol. 101, pp. 064106, March 2007.

[5] R. Xu, Y. Y. Zhu, S. Chen, F. Xue, Y. L. Fan, X. J. Yang, Z. M. Jiang, "Epitaxial growth of Er_2O_3 films on Si(0 0 1)," *J. Appl. Phys.*, vol. 277, pp. 496-501, February 2005.

[6] G. Kresse and J. Furthmüller, "Efficient iterative schemes for *ab* initio total-energy calculations using a plane-wave basis set," *Phys. Rev. B*, vol. 54, pp. 11169-11186, May 1996.

[7] G. Kresse and J. Furthmüller, "Efficiency of ab-initio total energy calculations for metals and semiconductors using a plane-wave basis set," *Mater. Sci.*, vol. 6, pp. 15-50, March 1996.

[8] G. Kresse and J. Furthmüller, "Norm-conserving and ultrasoft pseudopotentials for first-row and transition elements," *J. Phys.: Condens. Matter*, vol. 6, pp. 8245-8257, April 1994.

[9] G. Kresse and D. Joubert, "From ultrasoft pseudopotentials to the projector augmented-wave method," *Phys. Rev. B*, vol. 59, pp. 1758-1775, July 1999.

[10] J. P. Perdew, J. A. Chevary, S. H. Vosko, K. A. Jackson, M. R. Petersen, D. J. Singh, and C. Fiolhais, "Atoms, molecules, solids, and surfaces: Applications of the generalized gradient approximation for exchange and correlation," *Phys. Rev. B*, vol. 46, pp. 6671-6686, September 1992.

[11] P. L. Liu, A. V. G. Chizmeshya, and J. Kouvetakis, "First-principles studies of GaN(0001) heteroepitaxy on ZrB_2(0001)," *Phys. Rev. B*, vol. 72, pp. 245335, December 2005.

[12] X. Wang, Y. L. Zhu, M. Heb, H. B. Lu, and X. L. Ma, "Structural and microstructural analyses of crystalline Er_2O_3 high-k films grown on Si (0 0 1) by laser molecular beam epitaxy," *Acta Materialia*, vol. 59, pp. 1644-1650, December 2011.

Yen-Wei Chen is a graduate student of Graduate Institute of Precision Engineering at National Chung-Hsing University, Taiwan. He obtained his bachelor's degree at National Sun Yat-sen University at Kaohsiung, Taiwan. His research interests are focused on the thermodynamic and electronic properties of the heteroepitaxial systems.

Po-Liang Liu is an associate professor of Graduate Institute of Precision Engineering at National Chung-Hsing University, Taiwan. He obtained his Ph.D. at National Taiwan University of Science and Technology at Taipei, Taiwan. His current research interests include first-principles simulation of the structural, electronic and energetic properties of semiconductors, and the hydrogen storages.

Chun-Hsiang Chan is a graduate student of Graduate Institute of Precision Engineering at National Chung-Hsing University, Taiwan. He obtained his bachelor's degree at National Kaohsiung Marine University at Kaohsiung, Taiwan. His research interests are focused on the hydrogen storage properties of the carbon nanotubes.